SOURCE RUPTURE PROCESS OF THE MENTAWAI, INDONESIA EARTHQUAKE OF OCTOBER 25th, 2010, DETERMINED BY JOINT INVERSION OF TELESEISMIC BODY WAVE AND NEAR-SOURCE STRONG MOTION DATA

Iman Fatchurochman* **Supervisor: Yuji YAGI****
MEE10502

ABSTRACT

We investigated the source process of the 2010 Mentawai earthquake by joint inversion method using near source and teleseismic body-wave data. To perform a stable inversion, we applied smoothing constraints and determined their relative weights on the observed data using ABIC criterion. The teleseismic waveforms were windowed for 150 sec, band-passed between 0.001 and 1.0 Hz, and then integrated into displacement. The strong motion data were windowed for 250 sec, band-passed between 0.005 and 0.5 Hz, and then integrated into velocity. The re-sampling rate for both data set to be 0.25 sec. We estimated the fault area to be 190 × 70 km^2. The main source parameters are as follows: (strike, dip, rake) = (324^0, 10^0, 94.6^0); the depth of hypocenter 13.5 km; the seismic moment 5.814×10^{20} Nm (Mw 7.8); source duration 102 sec; and the maximum slip amounts to 3.9 m.

The source rupture process obtained probably can be divided into 2 stages. At stage 1, the rupture nucleated near the hypocenter and then propagated to the southwestward and broke the first asperity centering at 14 km from the epicenter. At stage 2, the rupture propagated to the northwestward and broke the second asperity which was centered about 78 km from the epicenter. Our total slip distribution is well consistent with the result of tsunami waveform analysis by Satake et al. (2011). This earthquake was categorized as a tsunami earthquake due to the long rupture duration and the generation of tsunami much larger than expected for its magnitude.

Keywords: 2010 Mentawai Earthquake, Source Process, Tsunami Earthquake, Joint Inversion.

1. INTRODUCTION

On October 25th, 2010, a tsunami earthquake with a moment magnitude of 7.7 occurred closed to Mentawai Island, Indonesia. The location of this earthquake is near the trench where the Indo-Australia Plate is subducted beneath the Eurasia Plate. Some researchers identify this earthquake as a tsunami earthquake because the duration of the rupture was excessive and it generated a tsunami that was much larger than expected for its seismic magnitude (Newman et al. 2011, Lay et al. 2011). According to USGS data, the Mentawai earthquake has moment magnitude Mw 7.7 and surface magnitude Ms 7.2. This disparity of Ms-Mw is also characteristic of tsunami earthquake (Kanamori and Kikuchi, 1993). We can classify the earthquake that generates a tsunami as tsunamigenic, while the tsunami earthquake is a special class of events that generate tsunamis much larger than expected for their surface waveform magnitude (Kanamori, 1972). To understand the mechanism of tsunami

*Indonesian Agency for Meteorology, Climatology and Geophysics (BMKG).
**Professor, Graduate School of Life and Environmental Sciences, University of Tsukuba, Japan.

earthquake, it is important to investigate the coseismic slip area of these great earthquakes using local and global seismic data set.

2. DATA

In this study, 33 teleseismic stations (IRIS-DMC) and 12 components of five strong motion stations (BMKG) were used to infer the source process of the Mentawai earthquake 2010. The teleseismic body wave waveforms were windowed for 150 sec with starting 10 sec before P-wave arrival, band pass filtered between 0.001 and 1.0 Hz, and then integrated into displacement with sampling time 0.25 sec. The near source data were windowed for 250 sec with starting 5 sec before P-wave arrival and band pass filtered between 0.005 and 0.5 Hz, and then integrated into velocity with sampling time 0.25 sec.

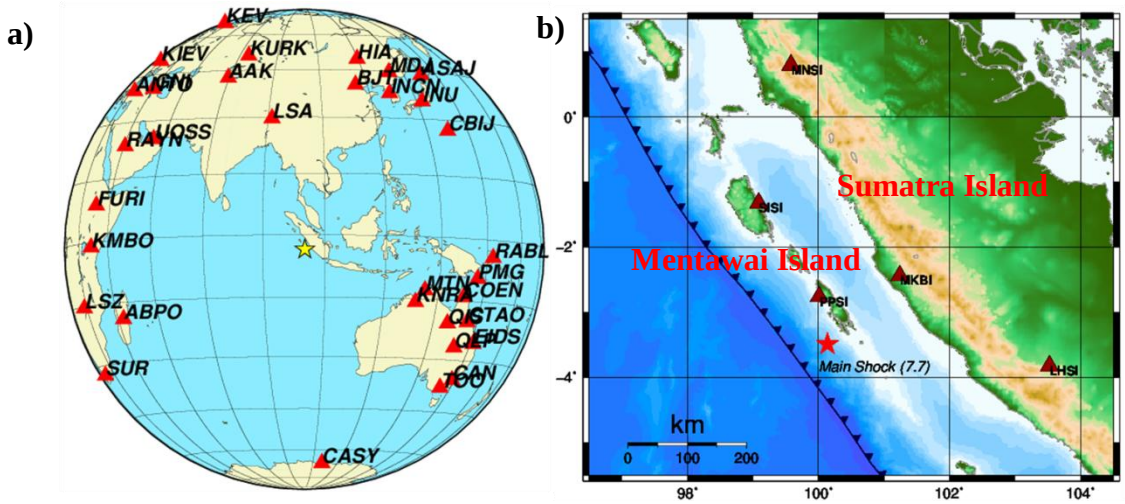

Figure 1. Station distribution is shown as a map view. The star represents the epicenter of the main-shock, red tringles indicate the stations. a) teleseismic network, b) strong motion network.

3. THEORY AND METHODOLOGY

To obtain the source process of the Mentawai earthquake, we analyzed the event using the standard fault parameterization. An inversion method was developed to infer earthquake rupture process from far-field and near source data set. The basic theory follows the standard waveform inversion scheme (Hartzell and Heaton, 1983) and numerical method developed by Yagi et al. (2004). The rupture process as a spatiotemporal slip distribution is represented on a fault plane. The fault plane is divided into $M \times N$ subfaults with length dx and width dy. Let $x_m = m\,dx$ and $y_n = m\,dy$. Slip rate functions on each subfault are described by a series of triangle functions with rise time τ and the fault slip vector described by K basis slip vectors. Using this source model, the observed seismic waveform at the station j is stated by:

$$W_j^{obs}(t_i) = \sum_{mnlk} X_{mnlk}\, g_{mnkj}\,(t_i - (l-1)\tau - T_{mn}) + e_j \qquad (1)$$

$$T_{mn} = \frac{\sqrt{x_m^2 + y_n^2}}{V} \qquad (2)$$

where X_{mnkl} is the k^{th} component of slip at the mn^{th} subfault with the l^{th} time step; $g_{mnkj}(t)$ is the green's function at the mn-subfault; T_{mn} is the start time of the basis function at each subfault and V is the rupture velocity; e_j is the Gaussian error with variance of σ_j. We calculate Green's function of

Table 1. Velocity structure (Kopp et al. 2001).

Vp (km/s)	Vs (km/s)	Density (10^3 Kg/m^3)	Q_p	Q_s	Thickness
For teleseismic body wave					
1.5	0	1.03			1
3	1.73	2.23			1
3.3	1.91	2.4			2
3.9	2.25	2.6			6
6.2	3.58	2.89			9
8.2	4.73	3.37			-
For strong ground motion					
3	1.73	2.23	260	130	2
3.3	1.91	2.4	300	150	2
3.9	2.25	2.6	400	200	6
6.2	3.58	2.89	800	400	9
8.2	4.73	3.37	1600	800	-

subfaults assuming the point source at the center of the subfaults. The sampling time of the Green's function was set at 0.25 sec, same with the observed waveform. The velocity structures assumed for theoretical teleseismic body wave and near source data calculation are based on the crustal structure of the central Sunda margin at the onset of oblique subduction (Kopp et al. 2001) as shown in table 1.

Generally, an increase in the number of model parameters may lead to give instability in the solution even a small change in the data resulting in a large change in the solution (Yagi et al. 2004). Considering the instability in the solution, we applied smoothing constraints to the slip distribution with respect to time and space to obtain more stable results. The smoothness constraint with respect to time is:

$$0 = X_{mnk\,(l-1)} - 2X_{mnkl} + X_{mnk\,(l+1)} + e_{t,} \qquad 2 \le l \le L\text{-}1 \tag{3}$$

where e_t is the Gaussian error. We can rewrite the equation (3) in the following simple vector form

$$\mathbf{0} = \mathbf{Tx} + \mathbf{e_t}, \tag{4}$$

where **T** is N_1 x N_a matrix ($N_1 = MN(L\text{-}2)K$). The smoothness constraint on the spatial distribution of total slip or smoothing constraint respect to space is introduced by a Laplacian finite difference operator:

$$0 = \sum_l \left[X_{(m-1)nkl} + X_{(m+1)nkl} + X_{m(n-1)kl} + X_{m(n+1)kl} - 4X_{mnkl}\right] + e_d \tag{5}$$

$$X_{0nkl} = X_{m0kl} = X_{(M+1)nkl} = X_{m(N+1)kl} = 0 \tag{6}$$

The equation (5) can be rewritten as follows:

$$\mathbf{0} = \mathbf{Dx} + \mathbf{e_d}, \tag{7}$$

where **D** is N_2 x N_a matrix ($N_2 = MNK$). To determine the model parameters that minimize the sum of square residual S from the observed data with two constraints, given by

$$S(\boldsymbol{x}, \sigma_j, \sigma_t, \sigma_d) = \sum_j \frac{1}{\sigma_j^2} \|\boldsymbol{y}_j - \boldsymbol{A}_j \boldsymbol{x}\|^2 + \frac{1}{\sigma_t^2} \|\boldsymbol{T}\boldsymbol{x}\|^2 + \frac{1}{\sigma_d^2} \|\boldsymbol{D}\boldsymbol{x}\|^2 \tag{8}$$

The values of σ_t and σ_d cannot be estimated directly, but σ_j can be estimated by the quality of data. To determine σ_t and σ_d objectively, we adopted the minimum Akaike's Bayesian information criterion (ABIC) (Akaike, 1980). The optimal ABIC for the present case is expressed using the following equation:

$$ABIC(\boldsymbol{x}, \sigma_t, \sigma_d) = \boldsymbol{N} \log S\left(\boldsymbol{x}, \sigma_j, \sigma_t, \sigma_d\right) - \log \left\| \frac{1}{\sigma_t^2} \boldsymbol{T^t T} + \frac{1}{\sigma_d^2} \boldsymbol{D^t D} \right\| + \log \left\| \sum_j \frac{1}{\sigma_j^2} A_j^t A_j + \frac{1}{\sigma_t^2} \boldsymbol{T^t T} + 1\sigma \boldsymbol{d2DtD} \right\| + C \tag{9}$$

N is the total number of the observation equations. We apply a grid-search method to obtain optimal values of σ_t and σ_d. We employed the non-negative least squares (NNLS) algorithm of Lawson and

Hanson (1974) to give positivity constraints on the model parameter. The positivity constraint is imposed not only because it is physically reasonable but also because negative slips lead to destructive interference between subfaults, producing unstable solutions (Hartzell and Heaton, 1983).

4. RESULTS AND DISCUSSION

4.1. Finite Fault Model

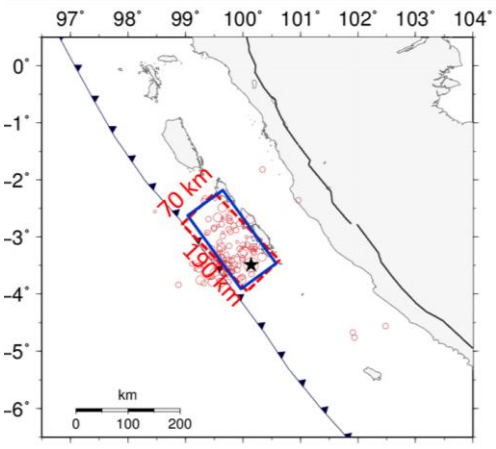

Figure 2. Geometry of the fault plane has slightly been modified from global CMT solution result.

Assuming that the faulting occurs on the single fault plane, we constructed the fault plane according to the aftershock distribution in a week after the mainshock and adjusted it to extend near to the seafloor as well. We then divided the fault plane into many subfaults and adopted the geometry of the focal mechanism from global CMT solution (strike, dip, rake) = (316^0, 8^0, 96^0) with slight modification to be consistent with the geometry of the plate boundary (Bird, 2003) as this result (strike, dip, rake) = (324^0, 10^0, 96^0) with the epicenter determined by BMKG (latitude = -3.49^0; longitude = 100.14^0). Figure 2 shows the geometry of the fault plane where the red rectangle denotes the geometry of global CMT solution result, while the blue rectangle denotes the geometry after being modified.

To obtain stable and detailed rupture process, we tried many lengths and widths of the fault plane. We finally constructed the fault plane with the area of 190 km × 70 km, the dimension of subfault 10 km^2 and the dip angle of 10^0 to cover the slip distribution of this earthquake, after many tries and errors.

Assuming that the earthquake occurred in interplate and considering the structure model and the dip angle, we adjusted the fault plane to extend near to the surface and we estimated the depth of hypocenter to be 13.5 km. The slip rate function of the subfault is expanded into a series of 15 triangle functions with a rise time of 2 sec. We also examined the optimum value for V_i within the range of 0.5 km/sec to 3.5 km/sec, and found that the maximum rupture velocity was 2.0 km/sec, which showed a minimum variance. The rigidity around the fault plane was assumed to be μ = 26.81 GPa from the structure model (Table 1).

4.2. Source Rupture Process

The inversion results are shown in Figure 3. Figures 3 (a), (b), (c) and (d) show the fault type, the source duration, the slip distribution and the comparison of observed with calculated waveforms of this earthquake, and Figure 4 shows the map view of slip distribution. Figure 3(a) illustrates the thrust fault type for this earthquake. The source time function (Figure 3b) indicates that a total seismic moment M_0 of 0.5814×10^{21} Nm (Mw 7.8) was released during a period of 102 sec. The total seismic moment estimated by this study is in agreement with global CMT moment solution, 0.677×10^{21} Nm (Mw 7.8). This result shows the anomalously long rupture duration comparing with those ordinary earthquakes with similar magnitude, such as the 1996 Peru earthquake (Mw 7.6 – 7.7), whose rupture duration is around 45 to 50 sec (Jennifer et al. 1999). Due to the excessive long rupture duration that reached 102 sec and generation of tsunami much larger than expected for its magnitude, the 2010 Mentawai earthquake is categorized as a tsunami earthquake. The final dislocation (Figure 3c) describes that the slip distribution extends along the dip direction. The rupture propagated from the hypocenter to the shallower subfaults. In asperity 1, the maximum slip is around 3.9 m, while in asperity 2 it is around 2.5 m.

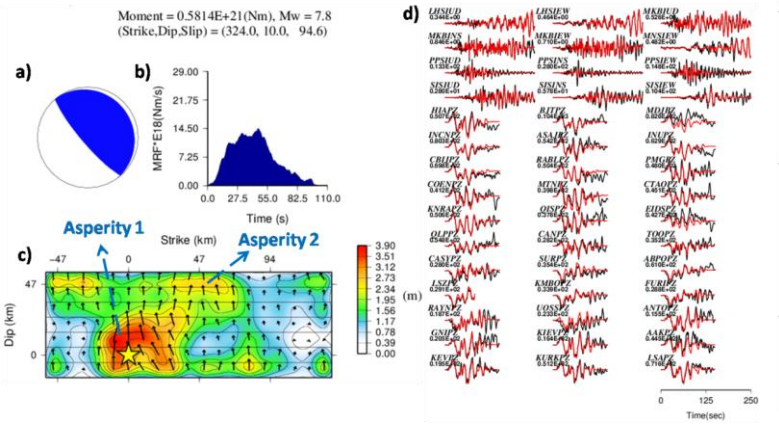

Figure 3. Joint inversion result of the Mentawai earthquake. a) Focal mechanism, b) source time function, c) slip distribution and d) comparison between observed (black) and calculated (red) waveforms

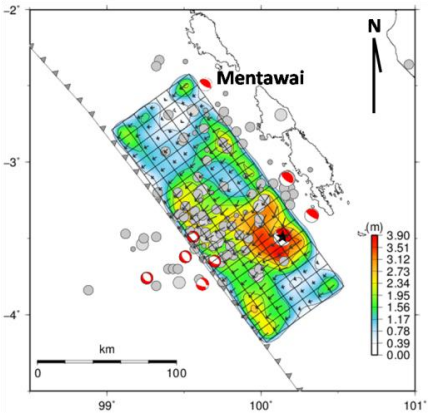

Figure 4. Distribution of coseismic slip on the map and aftershocks distribution in a week

This result is consistent with the maximum slip more than 3.0 m found by the result of tsunami waveform analysis (Satake et al. 2011). Our inversion result shows that in the shalower part, the slip ranges from 0.8 to 2.5 m, which is in the range of tsunami inversion result obtained by Satake et al. (2011). According to this proof, it probably can explain why this earthquake generated tsunami. However, our total slip distribution is different from the result of tele-seismic body wave analysis by Newman et al. (2011). They found the rupture was centered in one asperity with the maximum slip which was scaled from the original result to be 10 m, whereas our total slip distribution is well consistent with the result of tsunami waveform analysis by Satake et al. (2011).

Figures 3(d) shows the comparison between the observed (black curve) and the synthetic waveforms (red curve). Generally the waveforms show a good agreement between them except that the MNSI station located around 400 km north of the hypocenter is not fitting well. The discrepancy for this station may come from the assumed structure, which is not suitable for this station. According to this result, in general the assumed structure model we used seems to be suitable for all stations.

Figure 4 shows the map view of coseismic slip and aftershock distribution in a week after the mainshock. The aftershock data are obtained from BMKG while the focal mechanisms are taken from global CMT solution results. The rupture propagates mainly along the dip direction and the rupture area appears to extend parallel to the subduction zone between the Indo-Australia and Eurasia Plates. The focal mechanisms of the aftershocks as shown in Figure 4 predominantly are normal faulting near the trench. It probably describes the rupture of a locked subducted seamount on an otherwise decoupled zone, resulting in extension of the outer-rise causing the normal faulting aftershocks.

From the azimuthal view, the near source data only cover the epicenter from one side. Although this data set is not quite good especially in azimuthal coverage context, our result seems to have a good resolution. Probably this result may come from the advantage of the joint inversion of teleseismic body wave and strong motion data with an optimized ABIC. Fukahata et al. (2003) shows that optimized ABIC is particularly useful even with the insufficient observed data set.

The source rupture process obtained is probably divided into 2 stages. At stage 1, the rupture nucleated near the hypocenter and then propagated to the southwest direction and broke the first asperity centering at 14 km from the epicenter during 4 to 20 sec after the initial break. At this stage the maximum slip amounts to 3.9 meter at 20 sec after the initial break with the seismic moment of 2.359×10^{20} Nm (Mw = 7.5) which is smaller than the total seismic moment. At stage 2, the rupture propagated to the northwest direction and broke the second asperity which was centered about 78 km from the epicenter. The seismic moment for this asperity is 2.368×10^{19} Nm (Mw = 6.9).

5. CONCLUSIONS

By Joint Inversion method using the near source strong motion data obtained by BMKG and teleseismic data collected by IRIS-DMC, we estimated a detailed source model and slip distribution of the Mentawai, Indonesia earthquake of October 25th 2010. To perform a stable inversion, we applied smoothing constraints and determined their relative weights on the observed data using ABIC.

Assuming that the faulting occurs on the single fault plane, we constructed the fault plane according to the aftershock distribution in a week after the mainshock and adjusted it to extend near to the surface as well. We estimated the fault area to be 190 × 70 km^2. The main source parameters are as follows: (strike, dip, rake) = (324^0, 10^0, 94.6^0) and the depth of hypocenter 13.5 km. We obtained total seismic moment $Mo = 0.5814 \times 10^{21}$ Nm correspond to $Mw = 7.8$ with maximum slip amounting to 3.9 m at 14 km southwest of the epicenter. Source duration of this earthquake is around 102 sec.

The rupture process obtained is probably divided into 2 stages: the rupture nucleated around the hypocenter and propagated to the southwest and broke the first asperity centering at 14 km from the epicenter with maximum slip amounting to 3.9 m (stage I), then the rupture propagated to the northwest and the second asperity was broken, which was centered about 78 km from the epicenter (stage II). The rupture propagated mainly along the dip direction. We identify this earthquake as a tsunami earthquake in that it has characteristic of excessive long rupture duration and generated a tsunami that was much larger than expected for its magnitude. Our total slip distribution is well consistent with the result of tsunami waveform analysis by Satake et al. (2011).

6. RECOMMENDATION

The determination of source rupture process of tsunami earthquake is relatively difficult than ordinary earthquake. Some researchers found the result of slip distribution obtained by seismic inversion analysis was under estimation, comparing with the tsunami field observation. Therefore, we had better evaluate the slip distribution obtained by seismic inversion analysis as input for tsunami simulation model. We can explain the consistence of the seismic inversion analysis by comparing the synthetic waveforms obtained by tsunami simulation with the observed tsunami waveforms.

AKNOWLEDGEMENT

I would like to express my sincere gratitude to my advisor Dr. B. Shibazaki for his continuous support, valuable suggestion and guidance during my study.

REFERENCES

Akaike, H., 1980, pp. 143-166, University Press, Valencia, Spain.
Bird, P., 2003, Geochemistry Geophysics Geosystems, *4*(3), 1027, doi:10.1029/2001GC000252.
Fukahata, Y., Y. Yagi., and M. Matsu'ura., 2003, Geophys. Res. Lett., **30**, 10.1029/2002GL016293.
Hartzell, S. H. and T. H. Heaton., 1983, Bull. Seism. Soc. Am., **73**, 1553-1583.
J. L. Swenson and S. L. Beck., 1999, Pure appl geophys Volume 154, Numbers 3-4, 731-751
Kanamori, H., 1972, Phys.Earth Planet. Interiors, 6, 346-359.
Kanamori, H., M. Kikuchi., 1993, Nature, 361.
Kopp, H., et al., 2001, Geophys. J. Int, 147, 449-474.
Lawson, C. L. and R. J. Hanson., 1974, Prentice-Hall, Inc., Englewood Cliffs., New Jersey.
Lay, T., et al., 2011, Geophys. Res. Lett, 38 (6). Art. No. L06302 . ISSN 0094-8276
Newman, A. V., et al., 2011, Geophys. Res. Lett., 38, L05302, doi: 10.1029/2010GL046498.
Satake, K., et al., 2011, to be submitted to PAGEOPH 2011.
Yagi, Y., et al., 2004, Bull. Seism. Soc. Am., **94**, 1795-1807.